Rubidium-IV: A High Pressure Phase with Complex Crystal Structure

U. Schwarz
Max-Planck-Institut für Festkörperforschung, Heisenbergstrasse 1, 70569 Stuttgart, Germany
*and Max-Planck-Institut für Chemische Physik fester Stoffe, Pirnaer Landstrasse 176, 01257 Dresden, Germany**

A. Grzechnik, K. Syassen,† and I. Loa
Max-Planck-Institut für Festkörperforschung, Heisenbergstrasse 1, 70569 Stuttgart, Germany

M. Hanfland
European Synchrotron Radiation Facility, BP220, 38043 Grenoble, France
(Received 9 July 1999)

The crystal structure of the high-pressure phase rubidium-IV was investigated using synchrotron x-ray diffraction. Full profile refinements of angle-dispersive powder diffraction data resulted in a solution with the space group $I4/mcm$. The structure is made up of columns of face-sharing square antiprisms formed by one subset of Rb atoms (16 per unit cell). Quasi-one-dimensional channels in between these columns are occupied by a second subset of Rb atoms. These results demonstrate that a quite complex crystal structure is adopted by a heavy alkali metal during the progression of the pressure-driven electronic $s \rightarrow d$ transition. The structure of Rb-IV exhibits a close resemblance to the metal sublattice of the W_5Si_3-type structure.

PACS numbers: 61.50.Ks, 61.66.Bi, 62.50.+p, 64.70.Kb

With increasing pressure the heavy alkali metals lose their nearly free-electron character and at sufficiently high density they essentially become monovalent d transition metals. The pressure-driven $s \rightarrow d$ transition is believed to be the driving force for destabilizing the common highly symmetric low-pressure structures (bcc and fcc) with respect to lower symmetry structures [1]. The most detailed investigations of phase transitions in alkali metals have been performed for Cs, both experimentally (see Ref. [2] and literature cited therein) and theoretically (see, e.g., Refs. [1,3–5]). The sequence of high-pressure phase transitions of Rb shows an overall similarity to that of Cs. Rb transforms from the ambient pressure bcc phase to fcc (Rb-II) at 7 GPa [6]. Subsequent transitions to phases III–VI were detected by optical reflectivity measurements, electrical transport studies, and x-ray diffraction experiments [6–10]. The crystal structures of the phases Rb-V (20–48 GPa) and Rb-VI ($P > 48$ GPa) were determined [9,11] to be of the tetragonal Cs-IV-type [12] and the orthorhombic Cs-V-type [2], respectively. The appearance of Rb-VI roughly coincides with the end of the $s \rightarrow d$ transition [4]. The structures of the intermediate low-symmetry phases Rb-III (13–17 GPa) and Rb-IV (17–20 GPa) are unknown [10]. They occur in a compression range, where Cs has been reported to undergo an isostructural transition to the collapsed fcc phase Cs-III with only 0.2 GPa stability range [13] and where K transforms from fcc to an unidentified low-symmetry structure [10] which is characterized by strong optical absorption [14].

We report here a structure determination for the phase Rb-IV based on angle-dispersive synchrotron powder x-ray diffractometry. We have found a surprisingly complex structure, which has not been observed before for any elemental metal. The structure bears a close resemblance to the metal sublattice of the W_5Si_3-type structure. The observation of this very unusual structure type for Rb-IV has implications for developing a detailed picture of the electronic structure changes in heavy alkali metals during the progression of the $s \rightarrow d$ transition.

The diffraction experiments were carried out at the undulator beam line ID9 of the European Synchrotron Radiation Facility. The experimental setup was similar to that described earlier [2]. In short, the sample was compressed using a diamond anvil cell (DAC). The x-ray diffraction patterns (wavelengths near 0.45 Å) were recorded on a flat image plate. In order to improve powder averaging, the DAC was oscillated by $\pm 3°$. The images were converted to intensity vs 2Θ data using the FIT2D software [15]. Indexing, structure solution, and refinements were performed using the CSD [16] and GSAS [17] program packages. High purity Rb was obtained by a reaction of dried RbCl (+99.5%) with vacuum-heated Ca (+98.5%) and then purified by twofold destillation [18]. Liquid rubidium (melting point 39 °C) was filled into the gasket of the DAC under an oxygen-free dry argon atmosphere. A ruby chip served as the optical pressure sensor [19]. No pressure medium was used in order to avoid sample contamination. Diffraction diagrams were collected for different sample loadings in order to check the reproducibility of the results.

Figure 1(a) shows selected portions of diffraction diagrams measured for Rb-IV (16.9, 18.1, and 19.9 GPa) and at the Rb-IV to Rb-V transition (20.2 GPa). The full diffraction diagram of Rb-IV at 16.9 GPa is displayed in Fig. 1(b). All reflections of this pattern can be indexed on the basis of a cubic cell with $a_c \approx 10.35$ Å. However,

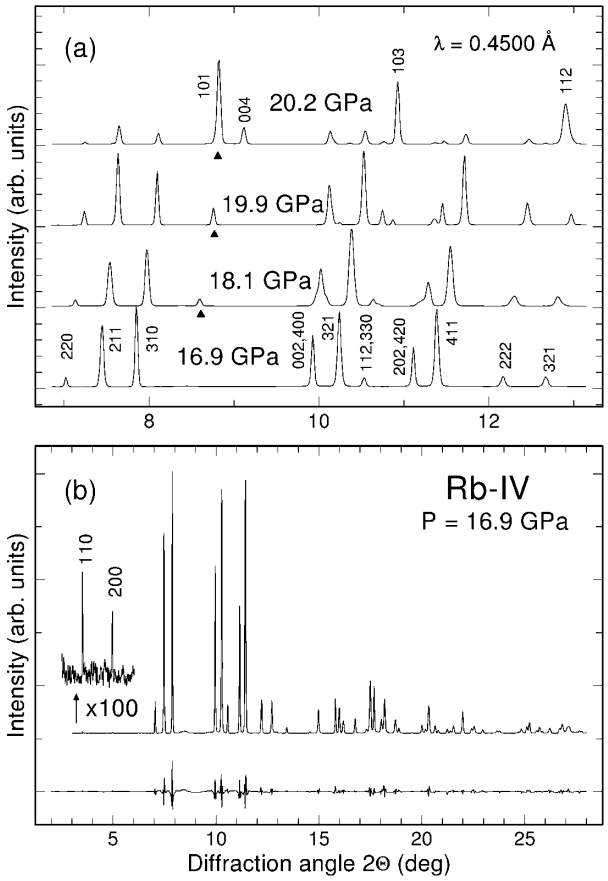

FIG. 1. (a) X–ray diffraction patterns of Rb at different pressures (selected angular range only). Miller indices in the lower and upper trace refer to the tetragonal unit cells of Rb-IV and Rb-V, respectively. (b) Full diffraction pattern of the phase Rb-IV at 16.9 GPa. The vertically expanded low-angle range demonstrates the presence of very weak reflections. The lower curve represents the difference between measured data and refined profile assuming half occupancy of $8g$ sites (see text). All diagrams are for a common x–ray wavelength (0.4500 Å), and the background was removed.

peak splittings at higher pressures [see Fig. 1(a)] indicate that the symmetry of the Rb-IV structure is lower than cubic. On the basis of a tetragonal unit cell with $a_c = a_t \approx 2 \times c_t$, 52 observed lines between $3° < 2\Theta < 25°$ can be indexed unambiguously. Corresponding lattice parameters and cell volumes of Rb-IV at selected pressures are given in Table I.

Some Rb-IV diagrams show a single extra peak near $2\Theta = 8.7°$ [marked by triangles in Fig. 1(a)], which does not fit to the basic tetragonal cell or simple supercells. Its position seems to shift continuously across the IV-V phase boundary near 20 GPa, where it becomes the (101) reflection of Rb-V. Thus, we tentatively attribute the extra peak in the Rb-IV diagrams to an admixture of Rb-V. Observing only the strongest Rb-V reflection (with low l index) would indicate a strong preferred orientation of Rb-V when embedded in Rb-IV.

We have also measured pressure-volume (PV) data for Rb-II and Rb-V, as shown in Fig. 2. An extrapolation of the fcc data into the Rb-IV range gives an upper bound for the atomic volume of Rb-IV which corresponds to 18.5 atoms per unit cell. Assuming 20 atoms per cell, the data points for the atomic volume of Rb-IV fall almost exactly on the extrapolated curve through the Rb-V data (see Fig. 2). The volume dependence of the c/a ratio of Rb-IV shown in the inset of Fig. 2 demonstrates that the c axis is slightly less compressible than the a axis.

The systematic extinctions for Rb-IV are compatible with the space groups (SG) $I4/mcm$, $I4cm$, and $I\bar{4}c2$. Thus, solutions of the crystal structure were performed in the centrosymmetric SG $I4/mcm$. Application of direct methods reveals that one type of Rb atoms occupies the Wyckoff positions $16k$ $(x, y, 0; x \approx 0.79, y \approx 0.08)$. The resulting arrangement of Rb(1) atoms (see Fig. 3) consists of columns of face-sharing square antiprisms which are interconnected by Rb(1)-Rb(1) contacts.

The Rb(1) framework hosts chains of a second type of Rb atoms as evidenced by electron density maxima in the difference Fourier map (see Fig. 4). Maxima occur at the $8g$ $(0.5, 0, z)$ positions, with appreciable density also at the $4b$ $(0.5, 0, 0.25)$ positions. Thus, the Fourier map in combination with the maximum possible number of 20 atoms per unit cell suggests two limiting Rb(2) arrangements, either full occupancy of $4b$ sites or a statistical occupation of $8g$ sites with an occupation factor of 0.5. These two structural models and a model with half occupancy of $8h$ sites were used as starting configurations for full profile refinements using GSAS [20]. Preferred orientation effects were taken into account using a spherical harmonics model [21].

The results of refinements for the pattern at 16.9 GPa are summarized in Table II. With Rb(2) in $4b$ or $8g$ sites,

TABLE I. Unit cell parameters for Rb-IV at selected pressures ($T = 298$ K). Errors are estimated standard deviations. The last column gives parameters for the phase Rb-V.

	Rb-IV	Rb-IV	Rb-IV	Rb-V
P (GPa)	16.9	18.1	19.9	20.2
a (Å)	10.3574(27)	10.2476(5)	10.0875(11)	3.0277(30)
c (Å)	5.1836(14)	5.16188(28)	5.1027(7)	11.328(17)
c/a	0.50047	0.503716	0.50584	3.7416
V_{cell} (Å^3)	556.07(3)	542.07(5)	519.24(11)	103.842

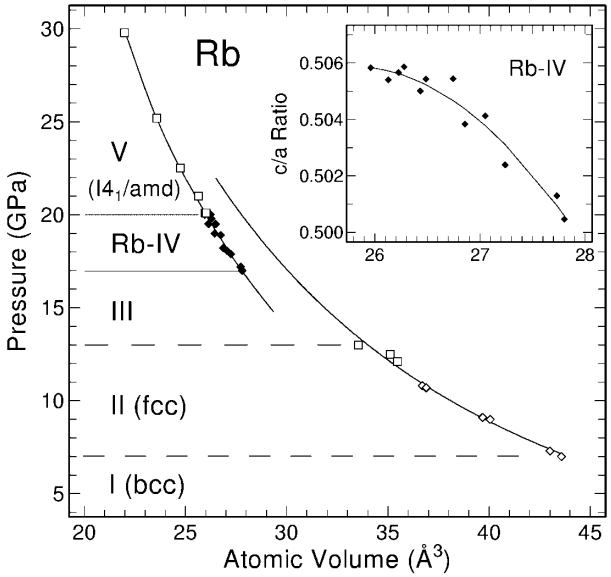

FIG. 2. Atomic volume of Rb as a function of pressure between 7 and 30 GPa. Phase transition pressures are marked by horizontal lines. Data points for Rb-II marked by open diamonds are from Ref. [6]. The data for Rb-IV are based on 20 atoms per unit cell (see text). The inset shows the c/a ratio of Rb-IV. All lines are guides to the eye.

we obtain very low values of $R(F^2)$ (residual for intensities), whereas the $R(F^2)$ value for the $8h$ case is significantly larger. This is also consistently found for other diffraction diagrams of Rb-IV, the reason being that intensities of several reflections cannot be well accounted for in the $8h$ model. For the $4b$ case the displacement parameter U is rather large. This indicates that the $4b$ site represents an average position for atoms centered around this site, in accordance with the Fourier map. Thus, among the three basic models tested, half occupancy of the $8g$ sites is considered to give the optimum description of the *average* Rb(2) atom arrangement.

The dark lines in Fig. 3 represent the shortest contacts (3.04 Å at 16.9 GPa) between Rb(1) atoms. This value is about 2 times the smallest tabulated ionic radius of Rb^+ (1.52 Å). The average distance between the Rb(2) atoms in the $8g$ sites is significantly smaller (2.59 Å). The channels occupied by Rb(2) are rather spacious and the structure may relax somewhat by forming zigzag or helical chains. There is, however, no indication in the Fourier map that such distortions are significant. Thus, due to the $s \rightarrow d$ transition we may have a very peculiar bonding situation which leads to extremely short metal-metal distances in the Rb-IV phase. Of course, a Rb-Rb separation 15% shorter than twice the smallest ionic radius would be difficult to accept without additional evidence or theoretical support.

We consider an alternative interpretation where the number of Rb(2) atoms in chain sites is less than four per unit cell. A refinement of the 16.9 GPa diagram,

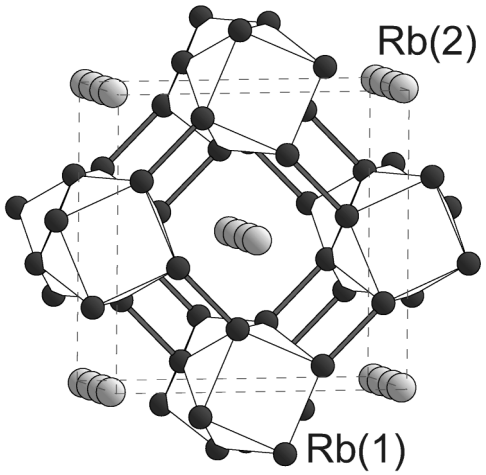

FIG. 3. The tetragonal structure of Rb-IV viewed approximately along the [001] direction. Note that, on average, the $8g$ chain sites of the Rb(2) atoms are at most half occupied (see text).

with occupation of both the $4b$ and $8g$ sites and with occupation factors treated as free parameters, converges to occupation numbers of 0.17 for $4b$ and 0.35 for $8g$, corresponding to 19.48 atoms per cell or an average chain atom separation of 2.97 Å. In view of the preferred orientation effects, this result may be considered an "over-refinement." However, it can possibly serve as a guide for theoretical structure optimizations in suitable supercells. In this context we note that we have not observed any supercell reflections. We do not rule out the possibility that the extra diffraction peak seen in some Rb-IV diagrams (see above) reflects a c-axis ordering of the chain atoms rather than an admixture of Rb-V.

There is a quite surprising resemblance of the proposed Rb-IV structure to the metal atom sublattice in the W_5Si_3-type structure [22–24]. For instance, in W_5Si_3 the $16k$ atom coordinates are very similar to those of Rb-IV [22]. The chains, however, are formed by metal atoms in $4b$ sites [22]. The spacings between metal

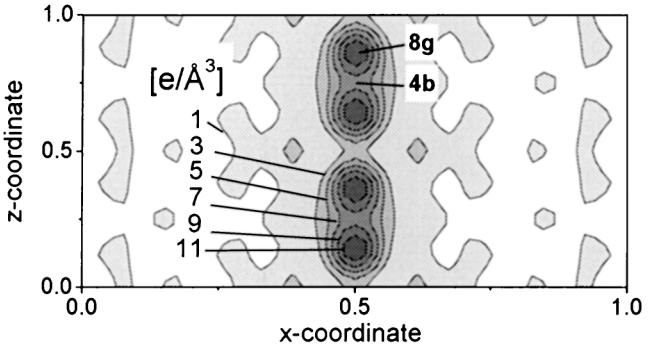

FIG. 4. Difference Fourier map of Rb-IV for a (010) plane. The x and z coordinates refer to the a and c axes of the tetragonal unit cell.

TABLE II. Results of structure refinements for Rb-IV at 16.9 GPa in space group $I4/mcm$. The Rb(1) atoms occupy the Wyckoff 16*k* sites. The Rb(2) atoms are assumed to occupy either 8*g*, 4*b*, or 8*h* positions, with half occupancy in the latter two cases. The displacement parameters U are in units of 100 Å^2. Errors refer to the estimated standard deviations of GSAS [17].

Parameter	8*g*	4*b*	8*h*
x (Rb-1)	0.7919(4)	0.7927(4)	0.7932(4)
y (Rb-1)	0.0843(6)	0.0877(5)	0.0763(4)
z (Rb-1)	0.5	0.5	0.5
U (Rb-1)	2.51	3.31	3.43
x (Rb-2)	0.5	0.5	0.5238(8)
y (Rb-2)	0.0	0.0	0.0238(8)
z (Rb-2)	0.1400(29)	0.25	0.0
U (Rb-2)	6.52	31.35	5.00
R (F^2)	0.059	0.070	0.151

ions in the 4*b* sites of many W_5Si_3-type compounds are about 10% shorter than the shortest distance between the 16*k* atoms or between atoms in the elemental metals. Thus, structure solutions with very short metal-metal distances are not specific to the Rb-IV case, but are also encountered in structural studies of related silicides *at ambient conditions*. There, the short distances have been attributed to *d*-orbital overlap [23] or a partial occupation of the metal atom chains [24]. We are not aware of any clear experimental evidence for supercell formation in binary silicides. Possible superstructures and incommensurability effects seem to have been considered only for ternary W_5Si_3-analogous alloys [25].

A close similarity was pointed out between the tetragonal Cs-IV-type structure and the arrangement of Th atoms in α-$ThSi_2$ [26]. Furthermore, the topology of calculated valence electron density maxima in Cs-IV [5] follows the arrangement of Si atoms in $ThSi_2$. Thus, one may speculate that the arrangement of electronegative Si atoms in W_5Si_3 may reflect the locations of electron density maxima in Rb-IV. In W_5Si_3, the Si atoms are located in the centers of the square antiprisms and in 8*h* sites.

In conclusion, we have determined the crystal structure of the phase Rb-IV based on high-resolution monochromatic synchrotron x-ray diffraction. The results demonstrate that the pressure-driven breakdown of the nearly free-electron character of a simple metal induces a phase transition to a rather complex structure. An intriguing feature is the close similarity of the tetragonal Rb-IV structure to the metal sublattice of W_5Si_3-type compounds. The present paper partly closes the gap in our knowledge about the phase transition sequence in heavy alkali metals during the progression of the $s \rightarrow d$ transition. We like to mention that new x-ray diffraction data taken for K-III indicate a structural motif closely related to that of Rb-IV [27]. Work on the structure determination of Rb-III is in progress.

We thank U. Oelke for technical assistance and F. Kögel for the preparation of highly purified rubidium metal. We acknowledge discussions with R. Nelmes, who later also kindly informed us that a structure with a space group similar to that of Rb-IV but fewer atoms in the basic unit cell occurs in Ba.

*Present address.
†Corresponding author.
†Email address: syassen@servix.mpi-stuttgart.mpg.de

[1] D. A. Young, *Phase Diagrams of the Elements* (University of California Press, Berkeley, CA, 1991).
[2] U. Schwarz *et al.*, Phys. Rev. Lett. **81**, 2711 (1998).
[3] S. G. Louie and M. L. Cohen, Phys. Rev. B **10**, 3237 (1974).
[4] A. K. McMahan, Phys. Rev. B **29**, 5982 (1984).
[5] O. K. Andersen *et al.* (unpublished).
[6] K. Takemura and K. Syassen, Solid State Commun. **44**, 1161 (1982).
[7] H. Tups, K. Takemura, and K. Syassen, Phys. Rev. Lett. **49**, 1776 (1982).
[8] J. Wittig, in *Superconductivity in d- and f-band Metals*, edited by W. Buckel and W. Weber (Kernforschungszentrum, Karlsruhe, 1982).
[9] H. Olijnyk and W. B. Holzapfel, Phys. Lett. **99A**, 381 (1983).
[10] M. Winzenick, V. Vijayakumar, and W. B. Holzapfel, Phys. Rev. B **50**, 12 381 (1994).
[11] U. Schwarz *et al.*, Solid State Commun. **112**, 319 (1999).
[12] K. Takemura, S. Minomura, and O. Shimomura, Phys. Rev. Lett. **49**, 1772 (1982).
[13] H. T. Hall, L. Merrill, and J. D. Barnett, Science **146**, 1297 (1964).
[14] K. Takemura and K. Syassen, Phys. Rev. B **28**, 1193 (1983).
[15] A. P. Hammersley *et al.*, High Press. Res. **14**, 235 (1996).
[16] L. G. Akselrud *et al.*, Mater. Sci. Forum **133–136**, 335 (1993).
[17] A. C. Allen and R. B. Von Dreele, Los Alamos National Laboratory Report No. LAUR 86-748, 1994.
[18] A. Simon, Z. Anorg. Allg. Chem. **395**, 301 (1973).
[19] G. J. Piermarini *et al.*, J. Appl. Phys. **46**, 2774 (1975); H. K. Mao, J. Xu, and P. M. Bell, J. Geophys. Res. **91**, 4673 (1986).
[20] Details of the refinement procedure were similar to those described in Ref. [11].
[21] See, e.g., L. B. McCusker *et al.*, J. Appl. Crystallogr. **32**, 36 (1999).
[22] B. Aronsson, Acta Chem. Scand. **9**, 1107 (1955).
[23] R. Berger, Acta Chem. Scand. A **31**, 223 (1977).
[24] D. T. Cromer, A. C. Lawson, and R. B. Roof, Acta Crystallogr. Sect. B **31**, 1756 (1975).
[25] I. Schewe-Miller and P. Böttcher, J. Alloys Compd. **183**, 98 (1992).
[26] H. G. von Schnering and R. Nesper, Angew. Chem., Int. Ed. Engl. **26**, 1059 (1987).
[27] K. Syassen *et al.* (unpublished).